Short title (50 characters): **Aggregates of hybrid cyanobacteria-tobacco Rubisco**

Correspondence:

Douglas J Orr

Lancaster University, Lancaster Environment Centre, Lancaster, LA1 4YQ, UK

Tel: +44 (0)1524 593476

Email: d.j.orr@lancaster.ac.uk

Hybrid cyanobacterial-tobacco Rubisco supports autotrophic growth and pre-carboxysomal aggregation

Douglas J. Orr[1]*, Dawn Worrall[1], Myat T. Lin[2], Elizabete Carmo-Silva[1], Maureen R. Hanson[2], Martin A. J. Parry[1]

[1] Lancaster Environment Centre, Lancaster University, Library Avenue, Lancaster, LA1 4YQ, UK.

[2] Department of Molecular Biology and Genetics, Cornell University, Ithaca, NY 14850, USA.

One Sentence Summary:

Cyanobacterial Rubisco large subunits form functional hybrids with tobacco small subunits and pro-carboxysome micro-compartments via the linker protein CcmM35 in absence of cognate small subunits.

Keywords: carboxysome, CCM, cyanobacteria, Rubisco, photosynthesis

FOOTNOTES:

List of author contributions:

MAJP, MRH, MTL & ECS conceived research. All authors designed experiments. DJO, DW & MTL performed the experiments and analyzed data. All authors contributed to writing the manuscript.

Funding

This work was funded by the UK Biotechnology and Biological Sciences Research Council (BBSRC) under grant number BB/I024488/1 to M.A.J.P. and the US National Science Foundation (NSF) under grant number EF–1105584 to M.R.H.

*Correspondence: Douglas J Orr (d.j.orr@lancaster.ac.uk)

Abstract

Much of the research aimed at improving photosynthesis and crop productivity attempts to overcome shortcomings of the primary CO_2 fixing enzyme Rubisco. Cyanobacteria utilize a CO_2 concentrating mechanism (CCM), which encapsulates Rubisco with poor specificity but relatively fast catalytic rate within a carboxysome micro-compartment. Alongside active transport of bicarbonate into the cell, and localization of carbonic anhydrase within the carboxysome shell with Rubisco, cyanobacteria are able to overcome the limitations of Rubisco via localization within a high CO_2 environment. As part of ongoing efforts to engineer a β-cyanobacterial CCM into land plants, we investigated the potential for Rubisco large subunits (LSU) from the β-cyanobacteria *Synechococcus elongatus* (Se) to form aggregated Rubisco complexes with the carboxysome linker protein CcmM35 within tobacco chloroplasts. Transplastomic plants were produced that lacked cognate SeRubisco small subunits (SSU) and expressed SeLSU in place of tobacco LSU, with and without CcmM35. Plants were able to form a hybrid enzyme utilizing tobacco SSU and the SeLSU, allowing slow autotrophic growth in high CO_2. CcmM35 was able to form large Rubisco aggregates with the SeLSU, and these incorporated small amounts of native tobacco SSU. Plants lacking the SeSSU showed delayed growth, poor photosynthetic capacity and significantly reduced Rubisco activity compared to both wild-type tobacco and lines expressing the SeSSU. These results demonstrate the ability of the SeLSU and CcmM35 to form large aggregates without the cognate SeSSU in planta, harboring active Rubisco that enables plant growth, albeit at much slower pace than plants expressing the cognate SeSSU.

Introduction

The need to produce sufficient food for a growing population requires increasing the productivity and efficiency of agriculture in order to increase yields by the estimated 70% that will be needed by 2050 (Lobell et al., 2009; Ray et al., 2012). Given its central role in crop growth and productivity, improving photosynthesis is one approach that has the potential to generate step-change improvements in crop yields and resource use efficiency (Long et al., 2006; Ort et al., 2015). One of the primary limitations to photosynthesis is the relative inefficiency of the central carbon fixing enzyme Rubisco (ribulose 1,5-bisphosphate carboxylase/oxygenase), in particular its lack of specificity for CO_2 versus O_2, which leads to the energetically costly photorespiratory cycle (Whitney et al., 2011; Carmo-Silva et al., 2015; Sharwood et al., 2016; Flamholz et al., 2019). Exemplifying this, at current atmospheric levels of CO_2 and O_2, Rubisco's tendency to oxygenate rather than carboxylate its substrate RuBP (ribulose 1,5-bisphosphate) is estimated to reduce yields by as much as 36% and 20% in US grown soybean and wheat, respectively (Walker et al., 2016). Recent work has shown that limiting the costs of photorespiration by increasing its efficiency can provide dramatic benefits to plant growth (South et al., 2019).

Synthetic biology approaches hold promise for improving a number of facets of photosynthetic efficiency in crop plants (Maurino and Weber, 2013; Erb and Zarzycki, 2016; Orr et al., 2017). One example is the introduction of CO_2-concentrating mechanisms (CCM's) into C_3 crops to increase CO_2 concentrations at the site of Rubisco, a strategy which is likely to dramatically reduce the propensity of Rubisco to carry out oxygenation reactions by creating an environment which favors the beneficial carboxylation reaction (Price et al., 2011; McGrath and Long, 2014; Hanson et al., 2016; Long et al., 2016). Significant research efforts are being invested in this area, with varying sources for the CCMs being engineered, such as C_4 (Hibberd et al., 2008; Langdale, 2011) and CAM (Borland et al., 2014; Yang et al., 2015) systems from plants, and the pyrenoid and carboxysome-based systems of algae and cyanobacteria, respectively (Rae et al., 2017; Mackinder, 2018).

The CCM employed by cyanobacteria uses a combination of factors to create a high CO_2 environment localized around Rubisco (Price et al., 2008; Hanson et al., 2016). Aggregation and encapsulation of Rubisco within a highly ordered icosahedral protein micro-compartment, or carboxysome, allows co-localization of Rubisco and carbonic anhydrase (CA) to convert HCO_3^- to CO_2 where it is needed, and permits the movement of key molecules while limiting CO_2 escape. Generating a high CO_2 environment is also facilitated by a complex system of inorganic carbon transporters on the cyanobacterial outer membrane that move either HCO_3- or CO_2 into the cytoplasm through active and passive mechanisms (Price, 2011). Modelling the incorporation of the various components of the CCM

into plants suggests that once a fully functioning system is established within a higher plant chloroplast, photosynthetic rates could be improved by as much as 60% (McGrath and Long, 2014). The resulting subsequent improvements in yield could facilitate a major change in crop productivity and resource use efficiency (Ort et al., 2015; Hanson et al., 2016).

Significant progress has been made during recent years to unravel the molecular mechanisms of CCMs involving either carboxysomes or pyrenoids. In *Synechococcus elongatus* PCC7942, which produces β-carboxysomes, the *ccmM* gene gives rise to two proteins: CcmM58 and CcmM35, the latter arising from an internal ribosomal entry site (Long et al., 2007; Long et al., 2010). CcmM35 possesses three tandem repeats of Rubisco small subunit-like domains, and was initially thought to interact with Rubisco by replacing small subunits (Long et al., 2011). However, recent experiments suggest that CcmM35 binds Rubisco without releasing the small subunits (Ryan et al., 2019). A recent structural study revealed that the interaction between CcmM35 and Rubisco leads to dramatic phase separation (Wang et al., 2019). This nucleation of Rubisco holoenzymes by CcmM35 represents a critical first step in the assembly of β-carboxysomes (Cameron et al., 2013). In the pyrenoid of Chlamydomonas, similar phase separation was also observed when the Rubisco and a repeat protein called EYPC1 interact (Wunder et al., 2018). Likewise, in α-carboxysomes, Rubisco holoenzymes interact with a highly disordered repeat protein called CsoS2 (Cai et al., 2015; Liu et al., 2018). In a recent breakthrough, Long and co-workers were able to assemble α-carboxysomes in tobacco chloroplasts by co-expressing Rubisco large and small subunit genes along with CsoS2 and a shell protein called CsoS1A from *Cyanobium marinum* PCC7001 (Long et al., 2018). In another study, the shell proteins of β-carboxysome transiently expressed in the chloroplasts of *Nicotiana benthamiana* were able to assemble structures similar to micro-compartments (Lin et al., 2014a).

Our previous work demonstrated that replacing the Rubisco large subunit gene in tobacco with the Rubisco large and small subunit genes from *Synechococcus elongatus* PCC7942 (Se) resulted in plants that can support photosynthetic growth under elevated CO_2 conditions (Lin et al., 2014b; Occhialini et al., 2016). When CcmM35 was co-expressed in tobacco chloroplasts, the heterologous Rubisco was observed in a large aggregate with an appearance resembling a separate liquid phase (Lin et al., 2014a). In a previous study performed by another group, when the tobacco *rbcL* gene was replaced with that from *Synechococcus* PCC6301, no Rubisco large subunit (LSU) was detected in the transformed plant (Kanevski et al., 1999), and it was thought that the cyanobacterial LSU could not assemble with plant small subunit (SSU) to form a functional enzyme.

Here we investigated the assembly and functioning of cyanobacterial Rubisco within higher plant

chloroplasts when the Se LSU is expressed either with or without CcmM35 in the absence of cognate cyanobacterial SSU. Analysis of transplastomic tobacco lines incorporating some cyanobacterial components but lacking the cognate SSU revealed that the Se LSU and CcmM35 are able to form large aggregates of Rubisco within tobacco chloroplasts. Though only low amounts of tobacco SSUs were present, the transplastomic lines characterized differed significantly in physiology and biochemistry from comparable lines that also co-expressed the cognate cyanobacterial SSU. Remarkably, albeit at slow rates, in the absence of the cognate small subunits, the hybrid cyanobacterial LSU-tobacco SSU expressed in tobacco chloroplasts with and without CcmM35 was active and supported plant growth.

Results

Cyanobacterial Rubisco large subunits can support carbon fixation in tobacco chloroplasts in the absence of cognate small subunits

We generated two transplastomic tobacco lines named SeL and SeLM35 by replacing in-frame the entire tobacco Rubisco large subunit gene with that from *Synechococcus elongatus* PCC7942 (Se). In the SeLM35 line, the *ccmM35* gene was introduced downstream of the *Se-rbcL* gene to be co-expressed from the same chloroplast genome locus (Fig. 1A). We used the same regulatory elements at intergenic regions as described in our previous work namely, a terminator, an intercistronic expression element (IEE) and a Shine-Dalgarno (SD) or ribosome binding site (Lin et al., 2014b; Occhialini et al., 2016). In contrast to our previous work, the new transplastomic lines do not possess a corresponding cyanobacterial Rubisco small subunit gene. The *aadA* selectable marker gene was incorporated into the same operon as the *Se-rbcL* gene in the SeL construct instead of a separate operon as in the SeLM35 construct. We obtained homoplasmic transformed shoots after two rounds of selection, and were able to transfer them to soil for growth under elevated CO_2 (9000 ppm). We collected seeds from two independent SeL lines and one SeLM35 line. Both DNA and RNA blots confirmed complete removal of the *Nt-rbcL* gene and its corresponding transcript in these plants (Fig. 1B, S1). We also analyzed the transcripts containing *Se-rbcL* and *ccmM35* genes in these lines together with SeLS and SeLSM35 lines generated in our previous study (Fig. S1). The RNA blots showed bands arising from incomplete processing of IEE as well as read-through transcription of the downstream *aadA* operon, consistent with our previous observations (Occhialini et al., 2016).

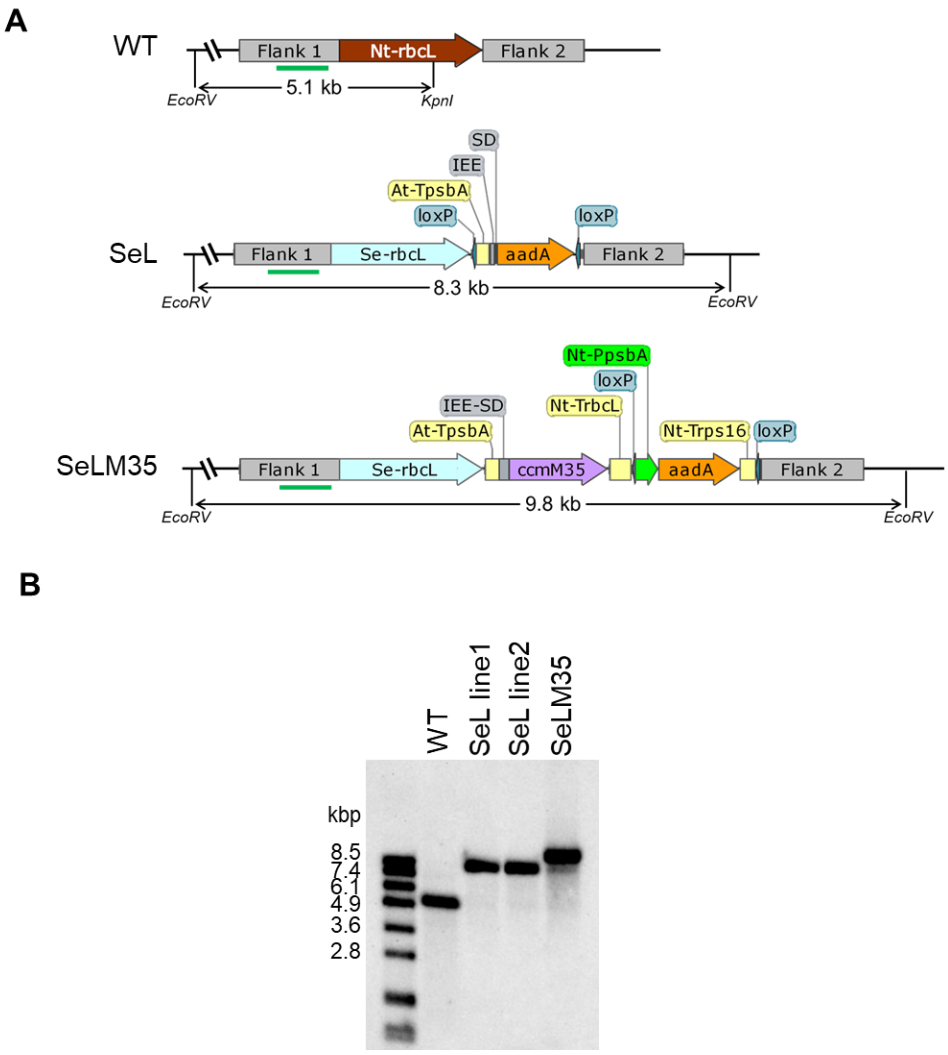

Figure 1. Replacement of the *rbcL* gene in tobacco chloroplasts with the *Se-rbcL* with or without the *ccmM35* gene. (A) The gene arrangements of wild-type (WT), SeL and SeLM35 tobacco lines along with the locations of the EcoRV and KpnI restriction sites used in the DNA blot. The binding site for the DIG-labeled DNA probe is shown in green bars. Seeds were obtained from two independent SeL lines and one SeLM35 line. (B) DNA blot analysis of the WT, SeL and SeLM35 samples digested with EcoRV and KpnI. All samples produced the expected band on the DNA blot.

Cyanobacterial Rubisco large subunits and CcmM35 aggregate in pro-carboxysome micro-compartments in tobacco chloroplasts

Expression of Se CcmM35 together with the cyanobacterial LSU in the SeLM35 transformant resulted in the formation of aggregates, or pro-carboxysome micro-compartments, in tobacco chloroplasts (Fig. 2). These aggregates were similar in size and shape to those observed in plants containing both the large and small subunits of Rubisco, and CcmM35 (SeLSM35, Fig. S2), but were absent from tobacco plants

166 expressing the Se LSU in the absence of CcmM35. Immuno-gold labelling confirmed the presence of the
167 Se LSU and CcmM35 proteins within the SeLM35 pro-carboxysome compartments (Fig. 2, S3, S4). In
168 comparison, in SeL plants, the Se LSU protein could be detected throughout the chloroplast and, as
169 expected, the anti-CcmM antibody gave only background level signal.
170 Gel electrophoresis and immunoblotting of leaf extracts demonstrated the presence of
171 cyanobacterial LSU and CcmM35 in SeLM35 transplastomic plants (Fig. 3). Visually, the two proteins
172 appear to be more abundant on a total soluble protein basis in these plants compared to SeLSM35. As
173 expected, both proteins were absent from WT leaf extracts, and in SeLS and SeL plants, Se LSU was
174 present but CcmM35 was not observed. The tobacco SSU was detected in WT, SeL and SeLM35 leaf
175 extracts, although its abundance in SeL was very low, and visualization of the ~13 kDa SSU required a
176 higher TSP load to detect clearly using immunoblotting (Fig. 3C). Non-denaturing native-PAGE suggested
177 that CcmM35 is present in functional complexes with Rubisco in the tobacco transplastomic lines
178 SeLSM35 and SeLM35 (Fig. 3B).

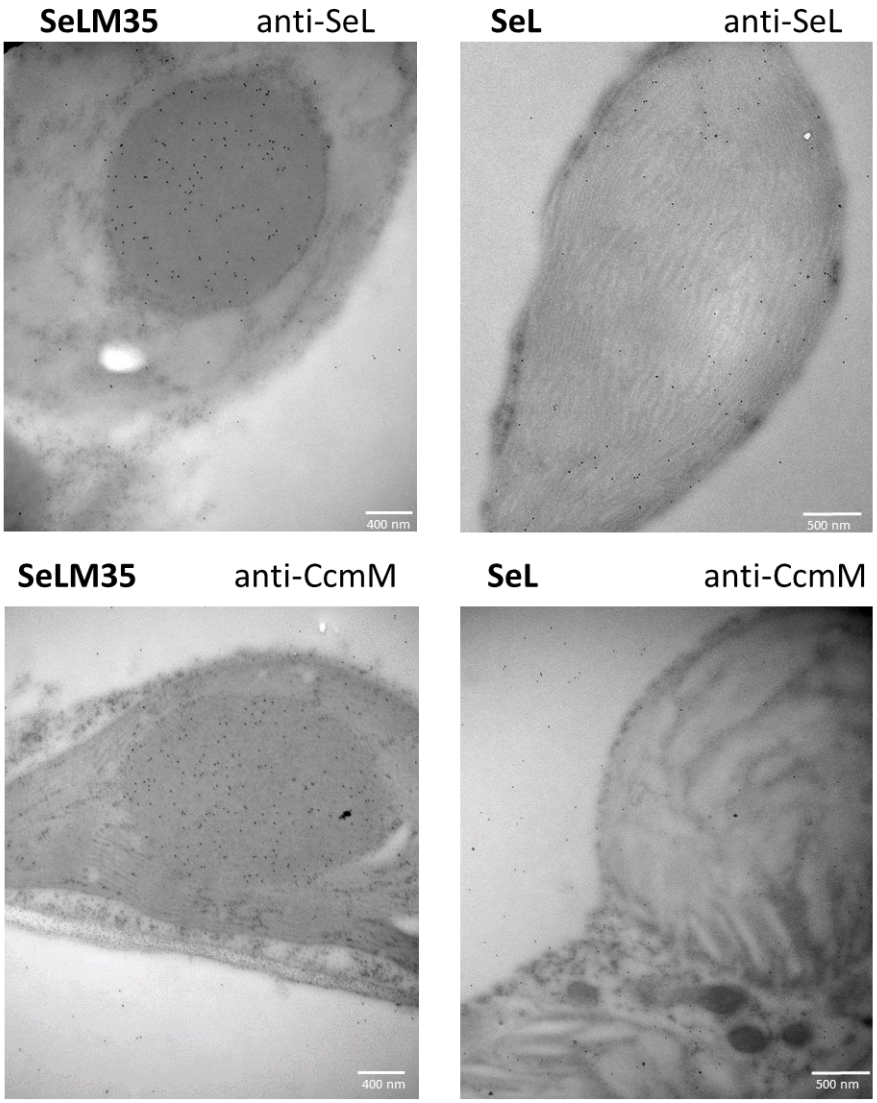

Figure 2. Tobacco plants expressing cyanobacterial Rubisco large subunits and CcmM35 contain a pro-carboxysome compartment in the chloroplast. Immunolocalization of *Synechococcus elongatus* (Se) proteins in the chloroplasts of transplastomic tobacco lines expressing the Rubisco large subunit and CcmM35 (SeLM35) or the large subunit alone (SeL). Electron micrographs of ultrathin sections of mesophyll cells probed with the indicated primary antibody and a secondary antibody conjugated to 10 nm gold particles. Scale bars indicate size. Additional images are presented in Supplemental Figures S3 and S4.

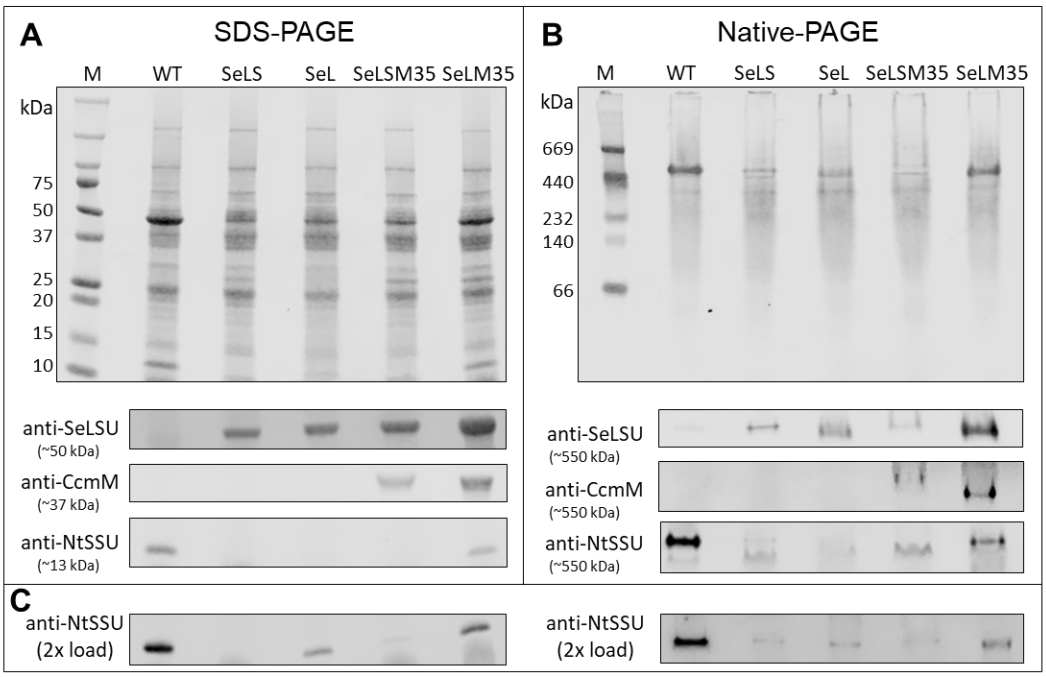

Figure 3. Protein composition of wild-type (WT) tobacco and transplastomic lines expressing β-cyanobacterial carboxysome components. Polypeptides in leaf extracts prepared from plants of each line were separated by denaturing SDS-PAGE (A) and non-denaturing Native-PAGE (B) and either stained with Coomassie Blue (upper panels) or used for immunoblotting with antibodies against cyanobacterial Rubisco large subunit (SeLSU) and CcmM35, and against tobacco Rubisco small subunit (NtSSU) (lower panels). Panels showing blotting of PAGE gels are slices from blots (see Fig. S5) that show the indicated size regions where the respective antibodies detect proteins of interest. For SDS-PAGE and Native-PAGE, 10 and 20 µg total soluble protein was loaded per lane, respectively. (C), SDS-Page and Native-PAGE gels immunoblotted with antibody against NtSSU, loaded with 20 and 40 µg total soluble protein, respectively.

Cyanobacterial Rubisco activity is impaired by the lack of a cognate SSU within tobacco chloroplasts

Consistent with previous efforts expressing Se Rubisco within tobacco chloroplasts, Rubisco content and activity on a leaf area basis were significantly lower in leaf extracts of all the transplastomic lines, representing less than 20% of the values in WT plants (Fig. 4). SeL plants in particular displayed minimal amounts of Rubisco. While Rubisco active sites in SeL were ca. 20% of SeLS plants expressing both Se Rubisco subunits (Fig. 4B), total activity in SeL was less than 5% of SeLS, and ca. 1% of WT tobacco, consistent with the extremely slow growth of these plants (see below). SeLM35 plants had significantly more Rubisco active sites than other transplastomic lines, including SeLSM35, which also expresses the CcmM35 linker protein (Fig. 4B, $P < 0.001$), although Rubisco total activity was not significantly different between the two lines (Fig. 4A, $P > 0.001$).

To ascertain the ability of tobacco chloroplasts to maintain active cyanobacterial Rubisco, we

212 determined Rubisco activation states from WT and transplastomic plants under steady state conditions.
213 As anticipated, WT plants were observed to have a comparatively low activation state in high CO_2
214 conditions (Fig. 4C). Lines expressing both Se Rubisco subunits, with or without CcmM35 showed
215 essentially fully active Rubisco. In contrast, in SeLM35 Rubisco, activation was ca. 70 %, and in SeL,
216 expressing just the cyanobacterial LSU, it was only ca. 20 %. These data indicate that these complexes,
217 although able to function, did not become fully active in these growth conditions.
218 All transplastomic lines displayed significantly lower total soluble protein compared to WT
219 tobacco (Fig. 4D, $P < 0.001$) and this decrease was largely consistent with the decreased amount of
220 Rubisco on an area basis (Fig. S6). Alongside reduced total soluble protein and Rubisco content and in
221 agreement with visual observation of these transplastomic plants, levels of chlorophyll a, b, and thus
222 total chlorophyll were significantly reduced (Fig. S7). Chlorophyll a was more severely reduced, and with
223 the exception of SeLS, all lines had a significantly reduced chlorophyll a/b ratio compared to WT tobacco.
224 Cyanobacterial Rubisco has been characterized to have a very high catalytic rate, but also a poor
225 affinity for CO_2 (high K_C value). In SeLS and SeLSM35 plants, values obtained for carboxylation rate, V_C,
226 and K_C, the Michaelis-Menten constant for CO_2, were consistent with previous work (Table 1; (Occhialini
227 et al., 2016). Rubiscos from SeLM35 and SeL, which contain the cyanobacterial LSU but lack a cognate
228 SSU, were able to carboxylate RuBP at significant rates. Immunoblotting suggested the presence of
229 tobacco SSU in the Rubisco complex, but this was likely at a stoichiometric ratio lower than 1:1 in
230 relation to the cyanobacterial LSU (Fig. 3). These two Rubisco enzymes had affinities for CO_2 comparable
231 to the enzyme from the transplastomic lines containing both the cyanobacterial LSU and SSU (Table 1).

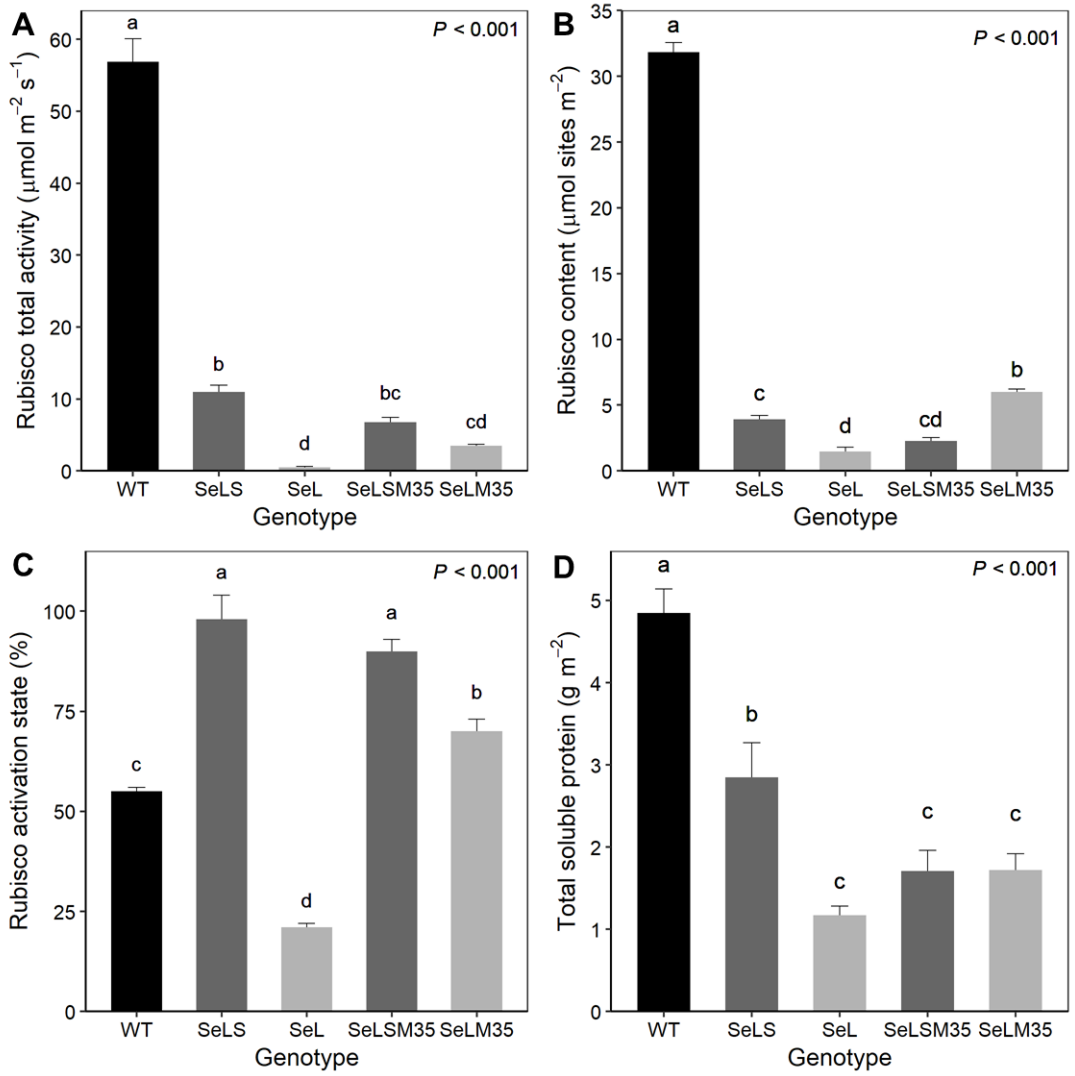

Figure 4. Rubisco and total soluble protein. Rubisco total activity (A), activation state (B), and content (C), and total soluble protein (D), of wild-type (WT) tobacco and transplastomic lines expressing β-cyanobacterial carboxysome components from *Synechococcus elongatus* (Se): Rubisco large subunit (L), Rubisco small subunit (S), CcmM35 (M35). Values represent mean ± SEM (n = 3-4 biological replicates). Letters denote significant differences ($P < 0.001$) as determined by Tukey's honestly significant difference [HSD] mean-separation test following ANOVA (*P*-values indicated on each panel).

Table 1. Rubisco catalytic properties. Maximum carboxylation rate (V_C), and Michaelis-Menten constant for CO_2 (K_C) of Rubisco from wild-type (WT) tobacco and transplastomic lines expressing β-cyanobacterial carboxysome components from *Synechococcus elongatus* (Se): Rubisco large subunit (L), Rubisco small subunit (S), CcmM35 (M35). Values represent mean ± SEM (n = 3-5 biological replicates). * Wild-type values from Occhialini et al. (2016). Letters denote significant differences ($P < 0.05$) between transplastomic lines as determined by Tukey's pairwise comparisons following ANOVA. For K_C differences were not significant at $P = 0.05$ level.

Line	V_C (μmol mg^{-1} min^{-1})	K_C (μM)
Wild-type*	3.9 ± 0.2	9.0 ± 0.3
SeLS	15.0 ± 0.9 a	168 ± 59 a
SeL	0.6 ± 0.2 b	105 ± 9 a
SeLSM35	10.9 ± 0.8 c	133 ± 12 a
SeLM35	2.0 ± 0.3 b	110 ± 22 a

The lack of a cognate Rubisco small subunit also impairs photosynthetic gas exchange

To evaluate the impact of the unusual Rubisco composition in the leaves of these transplastomic lines, gas exchange measurements were carried out. At the levels present in these transplastomic plants and in absence of a functional CO_2-concentrating mechanism, the faster catalytic rate of Se Rubisco does not confer an advantage in photosynthetic rate per leaf area even at 2000 ppm CO_2 (Fig. 5A). Consistent with previous work, aggregating cyanobacterial Rubisco through the expression of CcmM35 in SeLSM35 plants slightly reduced photosynthetic rates on an area basis (Fig 5A; Occhialini et al., 2016). SeLM35 photosynthetic rates show that the lack of the cognate Se SSU decreases photosynthetic rates even further (Fig. 5A). Most transplastomic lines showed a noticeable increase of photosynthesis under low oxygen conditions (Fig. S8). However, even at the highest CO_2 concentration measured combined with 2% oxygen, SeL plants displayed net photosynthetic rates that were barely above zero (Fig. S8C).

As a fully functional cyanobacterial CCM within tobacco will ideally require less Rubisco than wild-type plants, we also determined Rubisco content in the leaves used for gas exchange analyses. When CO_2 assimilation was normalized by Rubisco active site concentration, neither SeLM35 nor SeL outperformed WT plants even at 2000 ppm CO_2 (Fig 5B). Consistent with earlier work, at CO_2 levels well above ambient SeLS and SeLSM35 plants showed higher photosynthesis per Rubisco active site (Fig. 5B;(Occhialini et al., 2016)). Even accounting for very low Rubisco content, SeL plants show null normalized rates even at C_i of 2000 ppm CO_2 (Fig. 5B). This is consistent with the observation that even a

short exposure of several hours in ambient CO_2 conditions leads to tissue damage, and that even in growth conditions of 4000 ppm CO_2 SeL plants are extremely slow to develop (see below).

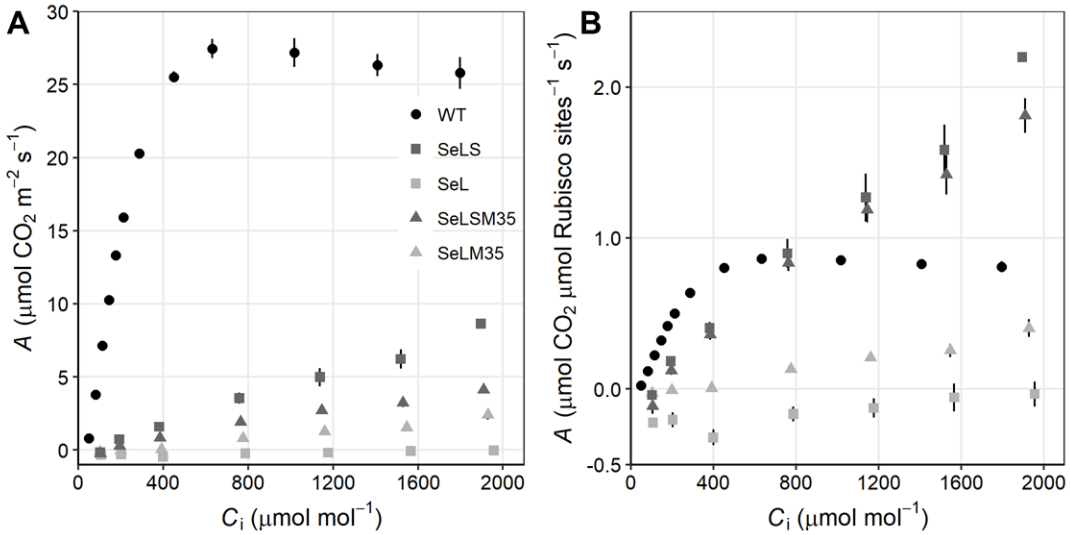

Figure 5. Response of leaf CO_2 assimilation to intercellular CO_2 concentrations (C_i). Rates are expressed on an area basis (A) and on a Rubisco active site basis (B) for leaves of wild-type (WT) tobacco and transplastomic lines expressing β-cyanobacterial carboxysome components from *Synechococcus elongatus* (Se): Rubisco large subunit (L), Rubisco small subunit (S), CcmM35 (M35). Values represent mean ± SEM (n = 3-4 biological replicates).

Replacement of tobacco Rubisco large subunits with cyanobacterial large subunits impairs growth irrespective of other components

Transplastomic plants where the native tobacco Rubisco large subunit (LSU) was replaced with the Se large subunit with or without the carboxysome linker protein CcmM35 (SeLSM35 and SeLM35) grew slowly even at 4000 ppm CO_2 when compared to both WT and lines expressing both Se Rubisco subunits (SeLS, Fig. 6A, S6, Table S2). Germination time was similar between all lines (~7 days). Plant height and total leaf area of SeLSM35 and SeLM35 plants started to visibly increase 60 days after sowing, and the growth rate for the subsequent 15 days was significantly slower in SeLM35 plants lacking the Se SSU compared to SeLSM35 ($P < 0.05$, Fig. 6B, 6C, Table S2). SeL plants expressing only the Se LSU were dramatically slower in growth ($P < 0.001$), which necessitated germination in tissue culture for establishment before transferring to soil. These plants took approximately three times as long as SeLS plants to reach a plant height of ~80 cm (Fig. 6B). SeL and SeLM35 plants produced numerous smaller leaves, consistent with the other line expressing CcmM35, SeLSM35 (Fig. S10). Both SeL and SeLM35

were noticeably paler than WT controls and transplastomic lines expressing the Se SSU (Fig. S7, S9, S10).

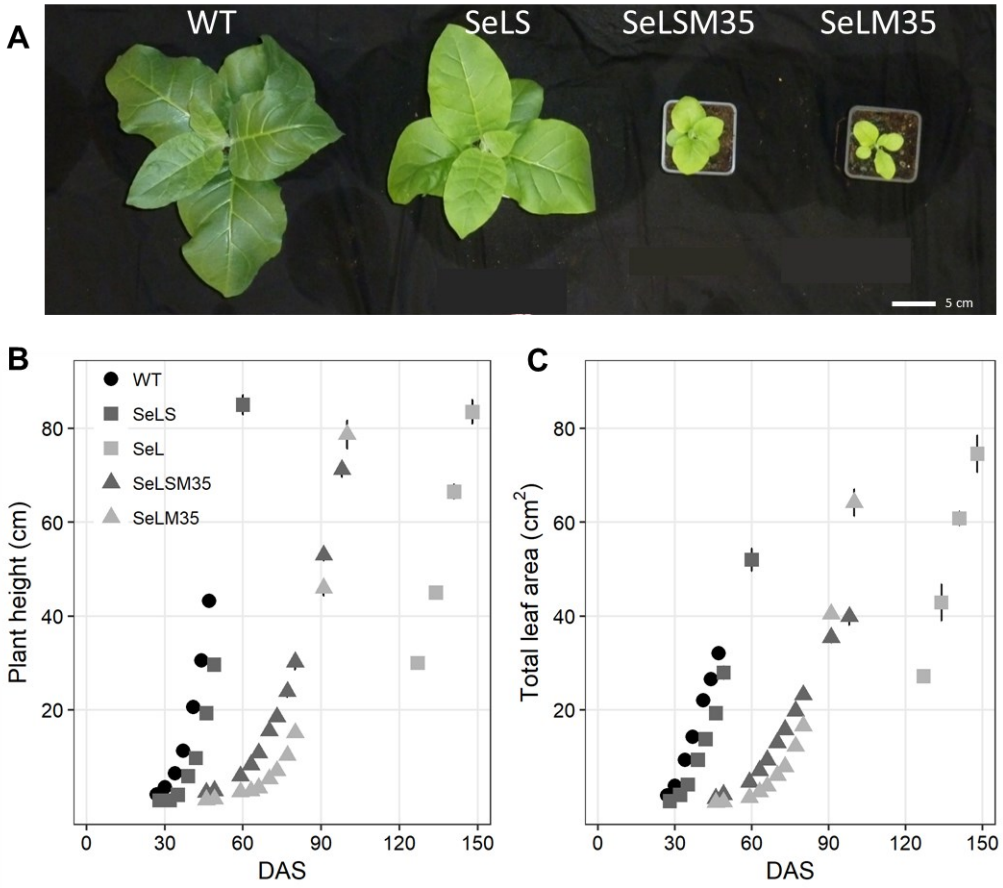

Figure 6. Plant development and growth traits. Photographs of 33 day old plants growing in parallel in the same growth conditions of 4000ppm CO_2 (A), plant height (B) and leaf area (C) development during the growth cycle of wild-type (WT) tobacco and transplastomic lines expressing β-cyanobacterial carboxysome components from *Synechococcus elongatus* (Se): Rubisco large subunit (L), Rubisco small subunit (S), CcmM35 (M35). Values represent mean ± SEM (n = 2-5 biological replicates). DAS, days after sowing.

Discussion

The current study describes two new transplastomic tobacco lines, namely SeL and SeLM35, where the native *rbcL* gene has been replaced with its cyanobacterial counterpart without the *Se-rbcS* gene. Previous work had shown the ability of L_8S_8 Rubisco from *Synechococcus elongatus* to assemble and function within higher plant chloroplasts and to form large aggregates of linked Rubisco complexes in the presence of CcmM35 (Lin et al., 2014a; Occhialini et al., 2016). Our current results show that cyanobacterial LSU interacts with the carboxysome linker protein CcmM35 in the absence of a cognate

cyanobacterial SSU, and forms pro-carboxysome-like aggregates in tobacco chloroplasts. In contrast to a previous study where no cyanobacterial LSU was detected in a similar tobacco transformant (Kanevski et al., 1999), we were able to detect the cyanobacterial LSU as well as catalytic activity of Rubisco in both SeL and SeLM35 lines (Table 1). It should be noted that the cyanobacterial LSU expressed in the previous study had the first 8 residues at its N terminus replaced by the first 11 residues of the tobacco LSU, possibly leading to lower stability of the modified LSU or inhibition of its assembly with the tobacco SSU (Kanevski et al., 1999).

Relative to comparable lines expressing Se SSU, both SeLM35 and SeL plants showed delayed growth (Fig. 6) and developed more numerous, but smaller leaves (Fig. S9, S10). SeL was not able to grow autotrophically from seeds even in high CO_2 levels, and required establishment on tissue culture media. Similar effects have been seen when engineering Rubisco in tobacco where either the introduction of a foreign LSU (Whitney and Andrews, 2001; Sharwood et al., 2008) or mutation of the native tobacco LSU (Whitney et al., 1999) leads to very low Rubisco amount and/or very poor activity.

Rubisco from both SeLM35 and SeL had dramatically slower maximum catalytic rates compared to the native Se enzyme (SeLS, Table 1), consistent with the slower growth of these plants. Combined with the significantly lower Rubisco active sites, this led to much lower Rubisco activity on a leaf area basis (Fig. 4). In both lines containing CcmM35, Rubisco catalytic rate was worse than that of β-cyanobacterial Rubisco extracted from SeLS where no aggregation occurs, which would suggest a putative negative impact of CcmM35 on Rubisco activity in the Se plants, and agrees with previous work with the SeLSM35 line (Occhialini et al., 2016). This is consistent with previous observations from plants expressing α-cyanobacterial Rubisco within a minimal α-carboxysome from *Cyanobium* (Long et al., 2018). The authors found that Rubisco catalytic rate was approximately halved when determined for Rubisco from tobacco chloroplasts; however, after high-speed centrifugation to remove insoluble carboxysomes, rates were consistent with those obtained from either the native cyanobacteria or expressed without linker proteins within tobacco. Movement of metabolites such as RuBP may be similarly inhibited by the formation of large β-pro-carboxysomes of LSU-CcmM35, as observed via K_{MRuBP} measurements made on tobacco derived minimal α-carboxysomes (Long et al., 2018). The large size of the observed pro-carboxysomes in SeLSM35 and SeLM35 plants, relative to native cyanobacterial carboxysomes, appears likely to have influenced metabolite movement. This highlights that an important part of balancing expression of the various components is not only to ensure correct formation of a functional carboxysome, but also to achieve a suitably sized microcompartment. However, Rubisco extracted from SeLM35 was significantly more active than the enzyme extracted from SeL plants,

showing that in the absence of Se SSU, CcmM35 helps sequester more tobacco SSU, possibly by increasing stability of the hybrid L_8S_8 enzyme or facilitating its assembly (Fig. 3).

The very low activity observed for SeL Rubisco that lacked the cognate SSU from cyanobacteria agrees with *in vitro* findings from a number of previous studies investigating the ability of LSU-only Rubisco to perform catalysis (Andrews and Ballment, 1984; Jordan and Chollet, 1985; Andrews, 1988). In studies including cyanobacterial Rubisco, *in vitro* preparations containing only L_8 octameric cores typically had detectable activity corresponding to only ~1% of the cyanobacterial holoenzyme, and even addition of heterologous higher plant SSU from spinach led to dramatic increases in activity (Andrews, 1988). The cyanobacterial L_8 core binds spinach SSU with an affinity an order of magnitude lower than its native SSU, and the activity of the hybrid enzyme was only half that of the enzyme with homologous subunits (Andrews and Lorimer, 1985). This suggests that the minimal activity observed for SeL Rubisco, ~5% of SeLS (Fig. 4), may in part result from a substoichiometric amount of tobacco SSU's binding to cyanobacterial L_8 cores.

A common theme in organization of Rubisco enzymes within both carboxysomes of photosynthetic bacteria and pyrenoids from green algae appears to be through interactions with a disordered repeat protein such as CcmM35 in β-carboxysomes, CsoS2 in α-carboxysomes and EPYC1 in pyrenoids (Long et al., 2011; Cai et al., 2015; Mackinder et al., 2016). In the case of β-carboxysomes and pyrenoids, the Rubisco enzymes were sequestered into a separate liquid phase by these linker proteins (Freeman Rosenzweig et al., 2017; Wunder et al., 2018; Wang et al., 2019). EPYC1 or CsoS2 were shown to interact only with the SSU (Liu et al., 2018; Atkinson et al., 2019), whereas both the large and small subunits are involved in binding CcmM35 based on a cryo-EM structural model, and the L_8 core alone was insufficient to form a separate liquid phase with CcmM35 (Wang et al., 2019). Thus, the tobacco SSUs are likely involved in the formation of CcmM35-Rubisco aggregates in SeLM35 plants although the stoichiometry between the Se LSU and tobacco SSUs was not determined. Indeed, the residues in Se SSU critical for interaction with CcmM35 are well conserved in tobacco SSU (Fig. S11; (Wang et al., 2019).

The poor photosynthetic performance of these transplastomic lines in the absence of a functional CCM with all the necessary components is unsurprising. However, the ability of some lines to outperform wild-type plants on a per Rubisco basis at higher CO_2 levels suggests that provided with high CO_2 concentrations such as those within a fully formed β-carboxysome shell in a complete CCM, the Rubisco levels within these plants may be sufficient to support improved rates of carbon assimilation. Consistent with this, Long and colleagues (2018) observed that leaf discs from plants expressing α-cyanobacterial Rubisco produced similar photosynthetic rates to wild-type tobacco plants in 2% (v/v) CO_2

conditions within a membrane inlet mass spectrometry system (MIMS). Thus, and even considering the associated nitrogen costs of producing the shell components, reducing the typically very large investment into Rubisco by C_3 plants may represent an overall nitrogen saving (McGrath and Long, 2014). An issue that is highly likely to be encountered when dealing with the numerous other components of the carboxysome shell is to optimize expression levels, and this may also be necessary for Rubisco. An increasing understanding of the role of chaperones for Rubisco assembly (Feiz et al., 2014; Salesse-Smith et al., 2018; Wilson and Hayer-Hartl, 2018; Conlan et al., 2019) may provide avenues to increase Se Rubisco amounts, should this become necessary to support the desired number of carboxysomes per chloroplast, in order to drive higher photosynthetic rates within a fully formed CCM. It is also possible that adjusting the chloroplast regulatory sequences used to express Se Rubisco subunits may be sufficient to increase the Rubisco amount.

The ability of CcmM35 to link Se LSU *in planta* without a cognate SSU shows that tobacco SSU can not only substitute Se SSU to form functional hybrid Rubisco, but can also result in an enzyme to which CcmM35 can bind. While the Se SSU does not appear to be essential for formation of a pro-carboxysome, the differences shown here based on its presence in a pro-carboxysome highlight its importance for full Rubisco functionality and carboxysome structural organization. These results support the likely necessity of co-engineering cognate subunits from a distant foreign Rubisco, as part of efforts to engineer both a foreign Rubisco into higher plants (Whitney and Andrews, 2001; Sharwood et al., 2008) and for more complex engineering of CO_2-concentrating mechanisms such as carboxysomes and pyrenoids from cyanobacteria and algae, respectively (Atkinson et al., 2016; Rae et al., 2017).

The carboxysome alone will be insufficient to attain higher rates of photosynthesis without the removal of existing stromal carbonic anhydrase and the addition of transporters to pump high levels of HCO_3^- into the chloroplast (Hanson et al., 2016; Long et al., 2018; Desmarais et al., 2019). There have been recent improvements in approaches to tackle the issue of localizing these inorganic carbon pumps (Rolland et al., 2016; Uehara et al., 2016), alongside advances in understanding the role of the various carbonic anhydrases (Hu et al., 2015; DiMario et al., 2016). Furthermore, there is now a better understanding of the actual ratios of components in β-carboxysomes (Sun et al., 2019), engineering of β-carboxysome shells to obtain cryoEM structural models (Cai et al., 2016; Sutter et al., 2019), an assembly of full β-carboxysomes in *E. coli* (Fang et al., 2018), and recent successes with α-carboxysomes (Long et al., 2018). These advances provide encouragement that ongoing research is steadily moving toward the ability to assemble these complex, powerful CCMs within plants to improve photosynthesis with the ultimate goal of improving global food security.

Materials and Methods

Construction of chloroplast transformation vectors

All primers used were obtained from Integrated DNA Technologies and listed in Table S1. Phusion™ high-fidelity DNA polymerase, FastDigest restriction enzymes and T4 DNA ligase from Thermo Scientific were used to generate amplicons, restriction digests and ligation products respectively. The ligation products were transformed into chemically competent DH5α *E. coli* and selected on LB agar medium with 100 µg/mL ampicillin. A template vector to hold each DNA piece was first constructed as follows. The aadA operon from BJF-070 vector (Hanson et al., 2013) was removed by self-ligation of the NsiI digest. An amplicon was generated from the resulting vector using NsiI-BJF3 and BamHI-BJF5 primers and ligated into the BamHI and NsiI sites of the vector to introduce SbfI and NotI sites upstream of the NsiI locus. The resulting vector, BJFE-BB, was used as a vector to hold each DNA element between the SbfI and NotI sites using BB-XXX-f and BB-XXX-r primers where 'XXX' stands for the name of each DNA element. Once ligated into the BJFE-BB vector, each DNA element was flanked by SbfI-MluI upstream and MauBI-NotI downstream. Since MluI and MauBI restriction sites have compatible cohesive ends, these DNA parts can be assembled in any desired order using an approach similar to the BioBrick method (Shetty et al., 2008). Specifically, we assembled an *aadA* module comprised of loxP-At_TpsbA-IEE-SD-RBS-aadA-loxP. We then modified pGEM-F1-rbcL-F2 vector described previously (Lin et al., 2014b) by introducing a SbfI site immediately downstream of the *Se-rbcL* gene. It was accomplished by ligating the amplicon generated with HindIII-LSUE5 and T1L-IEE3 primers into the HindIII and XbaI sites to obtain the pCT-rbcL-BB2 vector. Next, XbaI+AscI digest of the amplicon from TrbcL5 and AscI-LSUFl2r primers was ligated into XbaI and MluI sites of pCT-rbcL-BB2 vector to obtain pCT-rbcL-BB vector. Finally, we introduced the *aadA* module between the SbfI and NotI sites of pCT-rbcL-BB vector to obtain pCT-rbcL-BB-aadA vector used to generate the SeL chloroplast transformant tobacco line. pCT-rbcL-ccmM35 described previously (Lin et al., 2014b) was used in the generation of SeLM35 tobacco chloroplast transformant.

Generation of transplastomic tobacco plants

We introduced transformation vectors into two-week-old tobacco (*Nicotiana tabacum* cv. Samsun) seedlings with the Biolistic PDS-1000/He Particle Delivery System (Bio-Rad Laboratories) and tissue-culture based selection method as described previously (Occhialini et al., 2016). Briefly, about 10 µg of DNA was mixed with 100 µL of 50 mg/mL 0.6 µm gold nanoparticles, 100 µL of 2.5 M $CaCl_2$ and 40 µL of

0.1 M spermidine free-base by vortexing for about one minute. The gold particles were then pelleted in a microcentrifuge at 1000 rpm for 8 seconds and resuspended in 180 µL of 70% ethanol. After the washing of the gold particles was repeated one more time, the pellet was resuspended in about 60 µL of 100% ethanol and then spread on ten microcarrier discs used for bombardment. Two days later, the leaves from the bombarded seedlings were cut into halves and placed on RMOP agar medium with 500 µg/mL spectinomycin for 4-6 weeks at 23°C under 14 h light per day. The shoots arising were cut into 5 mm^2 pieces and subjected to a second round of selection on the same medium for another 4-6 weeks. The regenerated shoots were then transferred to MS agar medium for rooting and subsequently transferred to soil for growth in a chamber with elevated CO_2 (~9000 ppm) until the seeds were collected. Total DNA was extracted from leaf tissues using CTAB buffer, digested with EcoRV+KpnI restriction enzymes, separated on a 1% agarose gel, transferred to a Nylon membrane and detected with a DIG-label DNA probe as described previously (Lin et al., 2014b).

Analyses of transgenes' transcripts on RNA blots

The transcripts were analyzed on RNA blots using the procedure described previously with the same DIG-labeled RNA probes (Occhialini et al., 2016). Briefly, RNA samples were prepared from leaf tissues with a PureLink® RNA mini kit (Life Technologies) and their concentrations were estimated with a Qubit® RNA BR assay kit. About 1 µg each RNA sample was mixed with NorthernMax® formaldehyde load dye (Life Technologies) with 50 µg/mL ethidium bromide and incubated at 65 °C for 15 min before they were loaded to 1.3% agarose gel with 2% formaldehyde. After separation at 7 V cm^{-1} for about 2 h, the gel was washed three times in diethylpyrocarbonate-treated water for 10 min each and incubated in 20x SSC for 45 min before the RNAs were transferred to a positively charged nylon membrane under capillary action. The membrane was then exposed to UV radiation with a Stratalinker® UV Crosslinker, hybridized with 200 ng of each DIG-labeled RNA probe in ~ 4 mL of DIG EasyHyb buffer (Roche) at 68 °C overnight, and detected with anti-digoxigenin-AP antibody and CDP-Star chemiluminescent substrate (Roche).

Plant material

Seeds of wild type (WT) and transplastomic tobacco (*Nicotiana tabacum* cv. Samsun) were sown into trays of a commercial potting mix (Petersfield Products, UK) with a slow-release fertiliser (Osmocote, Scotts UK Professional, UK). Seedlings were thinned out after *ca.* two weeks, with individual plants transferred to 1 L pots after three weeks. Seeds of SeL were sown into tissue culture pots containing agar solidified MS medium containing 1% sucrose before transferring to soil after three weeks. Plants were

grown in a controlled environment chamber (Microclima 1750, Snijders Scientific B.V., Netherlands). The chamber was set at day/night temperatures of 24/22 °C with a 16 h photoperiod, 60 % humidity. The ambient CO_2 concentration within the chamber was maintained at 4000 ± 400 ppm using the integrated CO_2 controller. CO_2 levels were also monitored in the chamber with a Vaisala hand held GM70 meter (Vaisala, UK). Plants were kept well-watered. Space limitations within growth chambers necessitated growing plants in batches for growth analysis.

Fixation and embedding of plant tissue, immunogold labelling and TEM

Small pieces (1x1.5mm) of tissue from fully expanded leaves of plants equivalent in size to 33 DAS WT plants were incubated in fixative (4% paraformaldehyde, 2.5 % glutaraldehyde in 0.05 M sodium phosphate buffer pH 7.2) for 2 hours at room temperature with rotation. A vacuum was used to aid infiltration. After washing 3x 10 minutes in 0.05 M sodium phosphate buffer pH 7.2, the tissue was dehydrated in an ethanol series (50%, 70%, 80%, 90%) at room temperature for 30 minutes each step and finally 100% ethanol for 1 hour. Tissue was infiltrated with LR white resin (Agar Scientific, UK), first by incubating for 1 hour in 100% ethanol:LR white 1:1 (v/v), then for 2 hours in100% LR white and finally overnight in 100% LR white. Specimens were transferred to Eppendorf tubes charged with fresh 100% LR white resin. The tubes were sealed with plastic film and the resin polymerised at 50 °C for 16 hours.

Ultrathin sections (~90 nm) of embedded leaf material were captured on gold gilded grids (Agar Scientific, Stansted, UK) and used for immunogold labelling. Samples were blocked for 30 minutes in 1% BSA in phosphate buffered saline (PBS) and then incubated in primary antibody solution (antibody diluted 1/100 in 1% BSA in PBS) for 1.5 hours. Grids were washed 3x 10 minutes with 1% BSA in PBS before incubation for 1 hour with secondary goat anti-rabbit antibody conjugated to 10 nm gold particles (Agar Scientific, UK, 1/100 antibody dilution prepared in 1% BSA in PBS). Grids were washed 3x 10 minutes in 1% BSA in PBS and 3x 5 minutes in distilled water before air-drying. Images were obtained at 80kv using a JEOL 1010 (JEOL, Japan) microscope equipped with a digital AMT NanoSprint500 camera (Deben, UK).

Gel electrophoresis and immunoblotting

Soluble protein extracts were analysed for the presence of proteins via both denaturing (SDS-PAGE) and non-denaturing (Native-PAGE) gel electrophoresis. SDS-PAGE and immunoblotting was carried out as described in Perdomo *et al*. (2018) using Bio-Rad Mini-Protean TGX gels (Bio-Rad, UK). Non-denaturing gels were run using a Tris-glycine buffering system at 4°C as per the manufacturer's instructions. For both

types of electrophoresis, immunoblotting was as described by Perdomo *et al*. (2018) using SeLSU and CcmM antibodies described previously (Lin et al., 2014b) and a plant SSU antibody (Agri-Sera AS07 259, Agri-Sera, Sweden).

Rubisco biochemistry

Rubisco activities and activation state in leaf extracts were determined as described by Carmo-Silva *et al*. (2017), except that homogenate centrifugation was at a reduced 300 *g* for 1 min. Chlorophyll content in the homogenates was determined by the method of Wintermans and de Mots (1965) using ethanol and measuring absorbance in a microplate reader (SPECTROstar Nano, BMG LabTech, UK). Total soluble protein (TSP) in the same supernatant as used for Rubisco activity assays was determined via Bradford assay (1976). The amount of Rubisco was also quantified in the same supernatant by a [^{14}C]CABP [carboxyarabinitol-1,5-bisphosphate] binding assay (Whitney et al., 1999).

Rubisco catalytic properties were determined essentially as described previously (Prins et al., 2016; Orr and Carmo-Silva, 2018) with the following changes: leaf discs were ground in extraction buffer, followed by centrifugation at 300 *g* and 4°C for 1 min. Supernatants were immediately used for assays, which was previously found to be suitable with similar cyanobacterial Rubisco complexes (Lin et al., 2014b). Additional higher CO_2 concentrations (180, 280, and 410 µM) were also used for catalysis assays to enable determination of the Michaelis-Menten constant for CO_2 (K_M^{CO2} or K_C).

Photosynthesis measurements

Photosynthetic gas exchange was measured in healthy leaves that had recently reached full expansion, typically leaf 4 or 5 on plants of approximately 45 cm in height. A LI-6800F portable gas exchange system (LI-COR, Lincoln, NE, USA) was used to enclose a 6 cm^2 portion of leaf, with constant irradiance of 600 µmol photons m^{-2} s^{-1} supplied by the cuvette head LEDs, a vapour pressure deficit of 1.20 ± 0.03 kPa and a flow rate of 300 µmol m^{-2} s^{-1}. Leaf temperature was maintained at 24 ± 1°C. For all measurements, the entire gas exchange system was positioned inside the plant growth chamber, and controlled remotely via Ethernet connection. After the cuvette was clamped onto a leaf, the chamber door was kept closed to minimise fluctuations in CO_2 levels and the plant allowed to stabilise for at least 15 min at 3000 ppm CO_2 prior to commencing measurements. For transplastomic tobacco lines, the ambient CO_2 concentration (Ca) was subsequently decreased to 100 ppm, followed by increases to 200, 400, 800, 1200, 1600, 2000 and 2500 ppm CO_2. For wild-type tobacco, additional concentrations were used such that increases in CO_2 went from 50 to 100, 150, 200, 250, 300, 400, 600, 800, 1200, 1600, 2000 and 2500 ppm. For all

leaves measured, a separate CO_2 response curve was determined under 2% (v/v) O_2 conditions using a balanced air gas cylinder for input, using otherwise identical settings.

Plant biomass

Leaf numbers and leaf measurements were taken every 3-7 days from four or five individuals for each line (2 in the case of the SeL line). Plant height was measured from soil level to growing point. Measurements were initiated at 28 DAS for WT and SeLS, 46 DAS for SeLSM35 and SeLm35 and 127 DAS for SeL, due to the differing growth rates between lines and continued until the initiation of flowering. At the end of the growth period, final leaf measurements were taken and area measured using a LI-COR 3100 leaf area machine (LI-COR, Europe). Leaf areas were then derived for all time points.

Statistical analysis

Statistical differences between trait means were tested via one-way analysis of variance (ANOVA). In cases where an effect of genotype was observed ($P < 0.05$), a post-hoc Tukey test was used to conduct multiple pairwise comparisons. Statistical analyses were performed using RStudio (version 1.1.453, (R Studio Team, 2019)) and R (version 3.5.0, (R Core Development Team, 2013)). Plots were prepared with ggplot2 (Wickham, 2016). Plant height and leaf area data analyses involved fitting curves to the exponential phase of growth and comparing means of the curve coefficients using ANOVA. Where a significant difference was observed between lines, a post-hoc Holm-Sidak test was used for multiple pairwise comparisons. Analyses were performed in SigmaPlot (version 13, Systat Software, UK).

Accession Numbers

Sequence data for cyanobacterial RbcL and CcmM35 can be found in the GenBank data library under accession numbers AIM40198.1 and AIM40200.1 respectively.

Supplemental Data

Supplemental Figure S1. RNA blots of WT and transplastomic tobacco lines.

Supplemental Figure S2. Presence of pro-carboxysome compartments in tobacco transplastomic plants containing cyanobacterial Rubisco large subunits and CcmM35, with and without Rubisco small subunits.

Supplemental Figure S3. Electron micrographs of tobacco plants expressing cyanobacterial Rubisco large subunits and CcmM35 contain a pro-carboxysome compartment in the chloroplast.

Supplemental Figure S4. Additional examples of electron micrographs of tobacco plants expressing cyanobacterial Rubisco large subunits and CcmM35 with a pro-carboxysome compartment in the chloroplast.

Supplemental Figure S5. Western blots of SDS-PAGE and Native-PAGE gels used to examine protein composition of wild-type (WT) tobacco and transplastomic lines expressing β-cyanobacterial carboxysome components.

Supplemental Figure S6. Rubisco content expressed as grams per square metre.

Supplemental Figure S7. Chlorophyll content of transplastomic lines.

Supplemental Figure S8. Response of leaf CO_2 assimilation to intercellular CO_2 concentrations (Ci) under atmospheric levels and 2 % oxygen.

Supplemental Figure S9. Plant photographs at a comparable growth stage.

Supplemental Figure S10. Comparison of leaf size in transplastomic plants.

Supplemental Figure S11. Multiple sequence alignment of cyanobacterial and tobacco Rubisco small subunits.

Supplemental Table S1. Oligonucleotide sequences used in the construction of transformation vectors.

Supplemental Table S2. Plant growth data analyses.

Acknowledgments

We are thankful to Dr Sam Taylor (Lancaster) for support and advice with gas exchange measurements, and Nigel Fullwood (Lancaster) for guidance with TEM. We also thank the reviewers for helpful comments on the manuscript.

Tables

Table 1. Rubisco catalytic properties. Rubisco maximum carboxylation rate (V_C), and Michaelis-Menten constant for CO_2 (K_C) of wild-type (WT) tobacco and transplastomic lines expressing β-cyanobacterial carboxysome components from *Synechococcus elongatus* (Se): Rubisco large subunit (L), Rubisco small subunit (S), CcmM35 (M35). Values represent mean ± SEM (n = 3-5 biological replicates). * Wild-type values from Occhialini *et al.* (2016). Letters denote significant differences ($P < 0.05$) between transplastomic lines as determined by Tukey's pairwise comparisons following ANOVA.

Figure legends

Figure 1. Replacement of the *rbcL* gene in tobacco chloroplasts with the *Se-rbcL* with or without the *ccmM35* gene. (A) The gene arrangements of WT, SeL and SeLM35 tobacco lines along with the locations of the EcoRV and KpnI restriction sites used in the DNA blot. The binding site for the DIG-labeled DNA probe is shown in green bars. Seeds were obtained from two independent SeL lines and one SeLM35 line. (B) DNA blot analysis of the WT, SeL and SeLM35 samples digested with EcoRV and KpnI. All samples produced the expected band on the DNA blot.

Figure 2. Tobacco plants expressing cyanobacterial Rubisco large subunits and CcmM35 contain a pro-carboxysome compartment in the chloroplast. Immunolocalization of *Synechococcus elongatus* (Se) proteins in the chloroplasts of transplastomic tobacco lines expressing the Rubisco large subunit and CcmM35 (SeLM35) or the large subunit alone (SeL). Electron micrographs of ultrathin sections of mesophyll cells probed with the indicated primary antibody and a secondary antibody conjugated to 10 nm gold particles. Scale bars indicate size. Additional images are presented in Supplemental Figures S3 and S4.

Figure 3. Protein composition of wild-type (WT) tobacco and transplastomic lines expressing β-cyanobacterial carboxysome components. Polypeptides in leaf extracts prepared from plants of each line were separated by denaturing SDS-PAGE (A) and non-denaturing Native-PAGE (B) and either stained with Coomassie Blue (upper panels) or used for immunoblotting with antibodies against cyanobacterial Rubisco large subunit (SeLSU) and CcmM35, and against tobacco Rubisco small subunit (NtSSU) (lower panels). Panels showing blotting of PAGE gels are slices from blots (see Fig. S5) and show the indicated size regions where the respective antibodies detect proteins of interest. For SDS-PAGE and Native-PAGE, 10 and 20 µg total soluble protein was loaded per lane, respectively. (C), SDS-Page and Native-PAGE gels immunoblotted with antibody against NtSSU, loaded with 20 and 40 µg total soluble protein, respectively.

Figure 4. Rubisco and total soluble protein. Rubisco total activity (A), activation state (B), and content (C), and total soluble protein (D), of wild-type (WT) tobacco and transplastomic lines expressing β-cyanobacterial carboxysome components from *Synechococcus elongatus* (Se): Rubisco large subunit (L), Rubisco small subunit (S), CcmM35 (M35). Values represent mean ± SEM (n = 3-4 biological replicates).

643 Letters denote significant differences ($P < 0.05$) as determined by Tukey's honestly significant difference
644 [HSD] mean-separation test following ANOVA (*P*-values indicated on each panel).
645
646 **Figure 5. Response of net CO_2 assimilation (*A*) to intercellular CO_2 concentrations (C_i).** Rates are
647 expressed on an area basis (A) and on a Rubisco active site basis (B) for leaves of wild-type (WT) tobacco
648 and transplastomic lines expressing β-cyanobacterial carboxysome components from *Synechococcus*
649 *elongatus* (Se): Rubisco large subunit (L), Rubisco small subunit (S), CcmM35 (M35). Values represent
650 mean ± SEM (n = 3-4 biological replicates).
651
652 **Figure 6. Plant development and growth traits.** Photographs of 33 day old plants grown in parallel in
653 4000 ppm CO_2 (A), plant height (B) and leaf area (C) development during the growth cycle wild-type (WT)
654 tobacco and transplastomic lines expressing β-cyanobacterial carboxysome components from
655 *Synechococcus elongatus* (Se): Rubisco large subunit (L), Rubisco small subunit (S), CcmM35 (M35).
656 Values represent mean ± SEM (n = 3-5 biological replicates). DAS, days after sowing.
657
658

659 **References**

660

661 **Andrews TJ** (1988) Catalysis by cyanobacterial ribulose-bisphosphate carboxylase large subunits in the
662 complete absence of small subunits. J Biol Chem **263**: 12213–12219

663 **Andrews TJ, Ballment B** (1984) Active-site carbamate formation and reaction-intermediate-analog
664 binding by ribulosebisphosphate carboxylase/oxygenase in the absence of its small subunits. Proc
665 Natl Acad Sci U S A **81**: 3660–3664

666 **Andrews TJ, Lorimer GH** (1985) Catalytic properties of a hybrid between cyanobacterial large subunits
667 and higher plant small subunits of ribulosebisphosphate carboxylase-oxygenase. J Biol Chem **260**:
668 4632–4636

669 **Atkinson N, Feike D, Mackinder LCM, Meyer MT, Griffiths H, Jonikas MC, Smith AM, McCormick AJ**
670 (2016) Introducing an algal carbon-concentrating mechanism into higher plants: location and
671 incorporation of key components. Plant Biotechnol J **14**: 1302–1315

672 **Atkinson N, Velanis CN, Wunder T, Clarke DJ, Mueller-Cajar O, McCormick AJ** (2019) The pyrenoidal
673 linker protein EPYC1 phase separates with hybrid Arabidopsis–Chlamydomonas Rubisco through
674 interactions with the algal Rubisco small subunit. J Exp Bot. doi: 10.1093/jxb/erz275

675 **Borland AM, Hartwell J, Weston DJ, Schlauch KA, Tschaplinski TJ, Tuskan GA, Yang X, Cushman JC**
676 (2014) Engineering crassulacean acid metabolism to improve water-use efficiency. Trends Plant Sci
677 **19**: 327–338

678 **Bradford MM** (1976) A rapid and sensitive method for the quantitation of microgram quantities of
679 protein utilizing the principle of protein-dye binding. Anal Biochem **72**: 248–254

680 **Cai F, Bernstein SL, Wilson SC, Kerfeld CA** (2016) Production and characterization of synthetic
681 carboxysome shells with incorporated luminal proteins. Plant Physiol **170**: 1868–1877

682 **Cai F, Dou Z, Bernstein SL, Leverenz R, Williams EB, Heinhorst S, Shively J, Cannon GC, Kerfeld CA**
683 (2015) Advances in understanding carboxysome assembly in Prochlorococcus and Synechococcus
684 implicate CsoS2 as a critical component. Life **5**: 1141–1171

685 **Cameron JCJ, Wilson SSC, Bernstein SLS, Kerfeld CAC** (2013) Biogenesis of a Bacterial Organelle: The
686 Carboxysome Assembly Pathway. Cell **155**: 1131–1140

687 **Carmo-Silva E, Andralojc PJ, Scales JC, Driever SM, Mead A, Lawson T, Raines CA, Parry MAJ** (2017)
688 Phenotyping of field-grown wheat in the UK highlights contribution of light response of
689 photosynthesis and flag leaf longevity to grain yield. J Exp Bot **68**: 3473–3486

690 **Carmo-Silva E, Scales JC, Madgwick PJ, Parry MAJ** (2015) Optimizing Rubisco and its regulation for
691 greater resource use efficiency. Plant, Cell Environ **38**: 1817–1832

692 **Conlan B, Birch R, Kelso C, Holland S, De Souza AP, Long SP, Beck JL, Whitney SM** (2019) BSD2 is a
693 Rubisco-specific assembly chaperone, forms intermediary hetero-oligomeric complexes, and is
694 nonlimiting to growth in tobacco. Plant Cell Environ **42**: 1287–1301

695 **Desmarais JJ, Flamholz AI, Blikstad C, Dugan EJ, Laughlin TG, Oltrogge LM, Chen AW, Wetmore K,**
696 **Diamond S, Wang JY, et al** (2019) DABs are inorganic carbon pumps found throughout prokaryotic
697 phyla. Nat Microbiol. doi: 10.1038/s41564-019-0520-8

698 **DiMario RJ, Quebedeaux JC, Longstreth DJ, Dassanayake M, Hartman MM, Moroney J V.** (2016) The
699 cytoplasmic carbonic anhydrases βCA2 and βCA4 are required for optimal plant growth at low CO_2.

Plant Physiol **171**: 280–293

Erb TJ, Zarzycki J (2016) Biochemical and synthetic biology approaches to improve photosynthetic CO_2-fixation. Curr Opin Chem Biol **34**: 72–79

Fang Y, Huang F, Faulkner M, Jiang Q, Dykes GF, Yang M, Liu LN (2018) Engineering and modulating functional cyanobacterial CO2-fixing organelles. Front Plant Sci **9**: 739

Feiz L, Williams-Carrier R, Belcher S, Montano M, Barkan A, Stern DB (2014) A protein with an inactive pterin-4a-carbinolamine dehydratase domain is required for Rubisco biogenesis in plants. Plant J **80**: 862–869

Flamholz AI, Prywes N, Moran U, Davidi D, Bar-On YM, Oltrogge LM, Alves R, Savage D, Milo R (2019) Revisiting trade-offs between Rubisco kinetic parameters. Biochemistry **58**: 3365–3376

Freeman Rosenzweig ES, Xu B, Kuhn Cuellar L, Martinez-Sanchez A, Schaffer M, Strauss M, Cartwright HN, Ronceray P, Plitzko JM, Förster F, et al (2017) The Eukaryotic CO2-Concentrating Organelle Is Liquid-like and Exhibits Dynamic Reorganization. Cell **171**: 148–162.e19

Hanson MR, Gray BN, Ahner BA (2013) Chloroplast transformation for engineering of photosynthesis. J Exp Bot **64**: 731–742

Hanson MR, Lin MT, Carmo-Silva AE, Parry MAJ (2016) Towards engineering carboxysomes into C_3 plants. Plant J **87**: 38–50

Hibberd JM, Sheehy JE, Langdale JA (2008) Using C_4 photosynthesis to increase the yield of rice-rationale and feasibility. Curr Opin Plant Biol **11**: 228–231

Hu H, Rappel WJ, Occhipinti R, Ries A, Böhmer M, You L, Xiao C, Engineer CB, Boron WF, Schroeder JI (2015) Distinct cellular locations of carbonic anhydrases mediate carbon dioxide control of stomatal movements. Plant Physiol **169**: 1168–1178

Jordan DB, Chollet R (1985) Subunit dissociation and reconstitution of ribulose-1,5-bisphosphate carboxylase from *Chromatium vinosum*. Arch Biochem Biophys **236**: 487–496

Kanevski I, Maliga P, Rhoades DF, Gutteridge S (1999) Plastome engineering of ribulose-1,5-bisphosphate carboxylase/oxygenase in tobacco to form a sunflower large subunit and tobacco small subunit hybrid. Plant Physiol **119**: 133–141

Langdale JA (2011) C $_4$ Cycles: Past, Present, and Future Research on C $_4$ Photosynthesis. Plant Cell **23**: 3879–3892

Lin MT, Occhialini A, Andralojc PJ, Devonshire J, Hines KM, Parry MAJ, Hanson MR (2014a) β-Carboxysomal proteins assemble into highly organized structures in Nicotiana chloroplasts. Plant J **79**: 1–12

Lin MT, Occhialini A, Andralojc PJ, Parry MAJ, Hanson MR (2014b) A faster Rubisco with potential to increase photosynthesis in crops. Nature **513**: 547–550

Liu Y, He X, Lim W, Mueller J, Lawrie J, Kramer L, Guo J, Niu W (2018) Deciphering molecular details in the assembly of alpha-type carboxysome. Sci Rep **8**: 15062

Lobell DB, Cassman KG, Field CB (2009) Crop yield gaps: their importance, magnitudes, and causes. Annu Rev Environ Resour **34**: 179–204

Long BM, Badger MR, Whitney SM, Price GD (2007) Analysis of carboxysomes from *Synechococcus* PCC7942 reveals multiple rubisco complexes with carboxysomal proteins CcmM and CcaA. J Biol

740 Chem **282**: 29323–29335

741 **Long BM, Hee WY, Sharwood RE, Rae BD, Kaines S, Lim Y-L, Nguyen ND, Massey B, Bala S, von**
742 **Caemmerer S, et al** (2018) Carboxysome encapsulation of the CO2-fixing enzyme Rubisco in
743 tobacco chloroplasts. Nat Commun **9**: 3570

744 **Long BM, Rae BD, Badger MR, Price GD** (2011) Over-expression of the β-carboxysomal CcmM protein in
745 *Synechococcu*s PCC7942 reveals a tight co-regulation of carboxysomal carbonic anhydrase (CcaA)
746 and M58 content. Photosynth. Res. pp 33–45

747 **Long BM, Rae BD, Rolland V, Förster B, Price GD** (2016) Cyanobacterial CO_2-concentrating mechanism
748 components: Function and prospects for plant metabolic engineering. Curr Opin Plant Biol **31**: 1–8

749 **Long BM, Tucker L, Badger MR, Dean Price G** (2010) Functional cyanobacterial β-carboxysomes have an
750 absolute requirement for both long and short forms of the CcmM protein. Plant Physiol **153**: 285–
751 293

752 **Long SP, Zhu XG, Naidu SL, Ort DR** (2006) Can improvement in photosynthesis increase crop yields?
753 Plant, Cell Environ **29**: 315–330

754 **Mackinder LCM** (2018) The Chlamydomonas CO_2-concentrating mechanism and its potential for
755 engineering photosynthesis in plants. New Phytol **217**: 54–61

756 **Mackinder LCM, Meyer MT, Mettler-Altmann T, Chen VK, Mitchell MC, Caspari O, Rosenzweig ESF,**
757 **Pallesen L, Reeves G, Itakura A, et al** (2016) A repeat protein links Rubisco to form the eukaryotic
758 carbon-concentrating organelle. Proc Natl Acad Sci U S A **113**: 5958–5963

759 **Maurino VG, Weber APM** (2013) Engineering photosynthesis in plants and synthetic microorganisms. J
760 Exp Bot **64**: 743–751

761 **McGrath JM, Long SP** (2014) Can the cyanobacterial carbon-concentrating mechanism increase
762 photosynthesis in crop species? A theoretical analysis. Plant Physiol **164**: 2247–2261

763 **Occhialini A, Lin MT, Andralojc PJ, Hanson MR, Parry MAJ** (2016) Transgenic tobacco plants with
764 improved cyanobacterial Rubisco expression but no extra assembly factors grow at near wild-type
765 rates if provided with elevated CO_2. Plant J **85**: 148–160

766 **Orr DJ, Carmo-Silva E** (2018) Extraction of Rubisco to determine catalytic constants. Methods Mol. Biol.
767 Humana Press, New York, NY, pp 229–238

768 **Orr DJ, Pereira AM, da Fonseca Pereira P, Pereira-Lima ÍA, Zsögön A, Araújo WL** (2017) Engineering
769 photosynthesis: Progress and perspectives. F1000Research **6**: 1891

770 **Ort DR, Merchant SS, Alric J, Barkan A, Blankenship RE, Bock R, Croce R, Hanson MR, Hibberd JM, Long**
771 **SP, et al** (2015) Redesigning photosynthesis to sustainably meet global food and bioenergy
772 demand. Proc Natl Acad Sci U S A **112**: 8529–8536

773 **Perdomo JA, Sales CRG, Carmo-Silva E** (2018) Quantification of photosynthetic enzymes in leaf extracts
774 by immunoblotting. Humana Press, New York, NY, pp 215–227

775 **Price GD** (2011) Inorganic carbon transporters of the cyanobacterial CO_2 concentrating mechanism.
776 Photosynth. Res. pp 47–57

777 **Price GD, Badger MR, von Caemmerer S** (2011) The prospect of using cyanobacterial bicarbonate
778 transporters to improve leaf photosynthesis in C_3 crop plants. Plant Physiol **155**: 20–26

779 **Price GD, Badger MR, Woodger FJ, Long BM** (2008) Advances in understanding the cyanobacterial CO2-

concentrating- mechanism (CCM): Functional components, Ci transporters, diversity, genetic regulation and prospects for engineering into plants. J. Exp. Bot. pp 1441–1461

Prins A, Orr DJ, Andralojc PJ, Reynolds MP, Carmo-Silva E, Parry MAJ (2016) Rubisco catalytic properties of wild and domesticated relatives provide scope for improving wheat photosynthesis. J Exp Bot **67**: 1827–1838

R Core Development Team (2013) A language and environment for statistical computing. http://www.r-project.org/

R Studio Team (2019) RStudio Cloud: Integrated Development for R. https://www.rstudio.com/

Rae BD, Long BM, Forster B, Nguyen ND, Velanis CN, Atkinson N, Hee WY, Mukherjee B, Price GD, McCormick AJ (2017) Progress and challenges of engineering a biophysical carbon dioxide-concentrating mechanism into higher plants. J Exp Bot **68**: 3717–3737

Ray DK, Ramankutty N, Mueller ND, West PC, Foley JA (2012) Recent patterns of crop yield growth and stagnation. Nat Commun **3**: 1293

Rolland V, Badger MR, Price GD (2016) Redirecting the cyanobacterial bicarbonate transporters bica and sbta to the chloroplast envelope: Soluble and membrane cargos need different chloroplast targeting signals in plants. Front Plant Sci **7**: 185

Ryan P, Forrester TJB, Wroblewski C, Kenney TMG, Kitova EN, Klassen JS, Kimber MS (2019) The small RbcS-like domains of the β-carboxysome structural protein CcmM bind Rubisco at a site distinct from that binding the RbcS subunit. J Biol Chem **294**: 2593–2603

Salesse-Smith CE, Sharwood RE, Busch FA, Kromdijk J, Bardal V, Stern DB (2018) Overexpression of Rubisco subunits with RAF1 increases Rubisco content in maize. Nat Plants **4**: 802–810

Sharwood RE, Von Caemmerer S, Maliga P, Whitney SM (2008) The catalytic properties of hybrid rubisco comprising tobacco small and sunflower large subunits mirror the kinetically equivalent source rubiscos and can support tobacco growth. Plant Physiol **146**: 83–96

Sharwood RE, Ghannoum O, Whitney SM (2016) Prospects for improving CO_2 fixation in C_3-crops through understanding C_4-Rubisco biogenesis and catalytic diversity. Curr Opin Plant Biol **31**: 135–142

Shetty RP, Endy D, Knight TF (2008) Engineering BioBrick vectors from BioBrick parts. J Biol Eng **2**: 5

South PF, Cavanagh AP, Liu HW, Ort DR (2019) Synthetic glycolate metabolism pathways stimulate crop growth and productivity in the field. Science (80-) **363**: eaat9077

Sun Y, Wollman AJM, Huang F, Leake MC, Liu L-N (2019) Single-organelle quantification reveals stoichiometric and structural variability of carboxysomes Ddependent on the environment. Plant Cell **31**: 1648–1664

Sutter M, Laughlin TG, Sloan NB, Serwas D, Davies KM, Kerfeld CA (2019) Structure of a synthetic beta-carboxysome shell. Plant Physiol pp.00885.2019

Uehara S, Adachi F, Ito-Inaba Y, Inaba T (2016) Specific and efficient targeting of cyanobacterial bicarbonate transporters to the inner envelope membrane of chloroplasts in arabidopsis. Front Plant Sci **7**: 1–8

Walker BJ, VanLoocke A, Bernacchi CJ, Ort DR (2016) The costs of photorespiration to food production now and in the future. Annu Rev Plant Biol **67**: 107–129

Wang H, Yan X, Aigner H, Bracher A, Nguyen ND, Hee WY, Long BM, Price GD, Hartl FU, Hayer-Hartl M (2019) Rubisco condensate formation by CcmM in β-carboxysome biogenesis. Nature **566**: 131–135

Whitney SM, Andrews TJ (2001) Plastome-encoded bacterial ribulose-1,5-bisphosphate carboxylase/oxygenase (RubisCO) supports photosynthesis and growth in tobacco. Proc Natl Acad Sci U S A **98**: 14738–14743

Whitney SM, Von Caemmerer S, Hudson GS, Andrews TJ (1999) Directed mutation of the Rubisco large subunit of tobacco influences photorespiration and growth. Plant Physiol **121**: 579–588

Whitney SM, Houtz RL, Alonso H (2011) Advancing our understanding and capacity to engineer nature's CO_2-sequestering enzyme, Rubisco. Plant Physiol **155**: 27–35

Wickham H (2016) ggplot2: Elegant graphics for data analysis using the grammar of graphics. Springer-Verlag New York

Wilson RH, Hayer-Hartl M (2018) Complex chaperone dependence of Rubisco biogenesis. Biochemistry **57**: 3210–3216

Wintermans JFGM, De Mots A (1965) Spectrophotometric characteristics of chlorophylls a and b and their phenophytins in ethanol. BBA - Biophys Incl Photosynth **109**: 448–453

Wunder T, Cheng SLH, Lai SK, Li HY, Mueller-Cajar O (2018) The phase separation underlying the pyrenoid-based microalgal Rubisco supercharger. Nat Commun **9**: 5076

Yang X, Cushman JC, Borland AM, Edwards EJ, Wullschleger SD, Tuskan GA, Owen NA, Griffiths H, Smith JAC, De Paoli HC, et al (2015) A roadmap for research on crassulacean acid metabolism (CAM) to enhance sustainable food and bioenergy production in a hotter, drier world. New Phytol **207**: 491–504